Electronic Supplementary Material (ESI) for RSC Advances.

Support Information

Synthesis of flowerlike carbon nanosheets from hydrothermally carbonized glucose: An in situ self-generating template strategy

Yun Chen, Wenge Qiu, Jiayuan Sun, Shining Li, Guangmei Bai, Shenghua Li, Chenghui Sun, Siping Pang

Additional Figures and Data

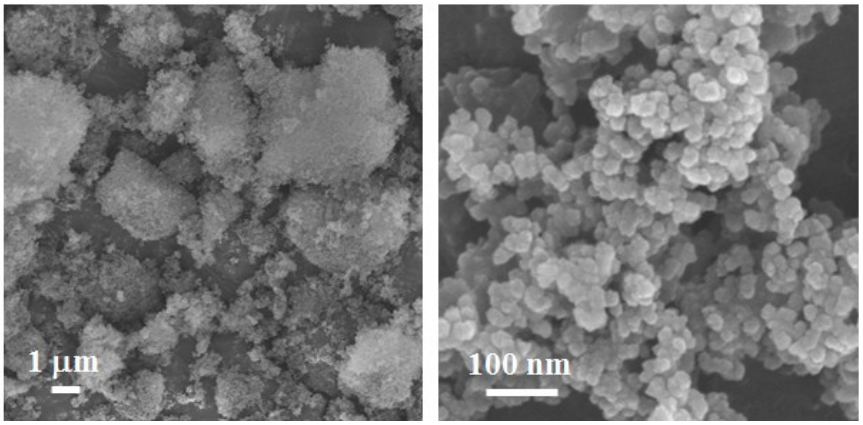

Fig. S1 SEM images of raw SiO_2 powder at different magnifications.

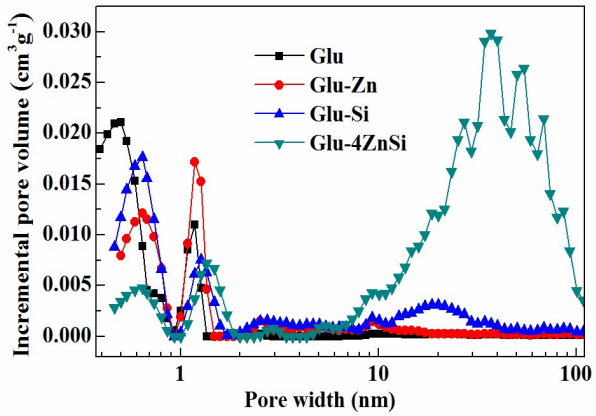

Fig. S2 Pore size distributions (PSD) of the resultant carbons.

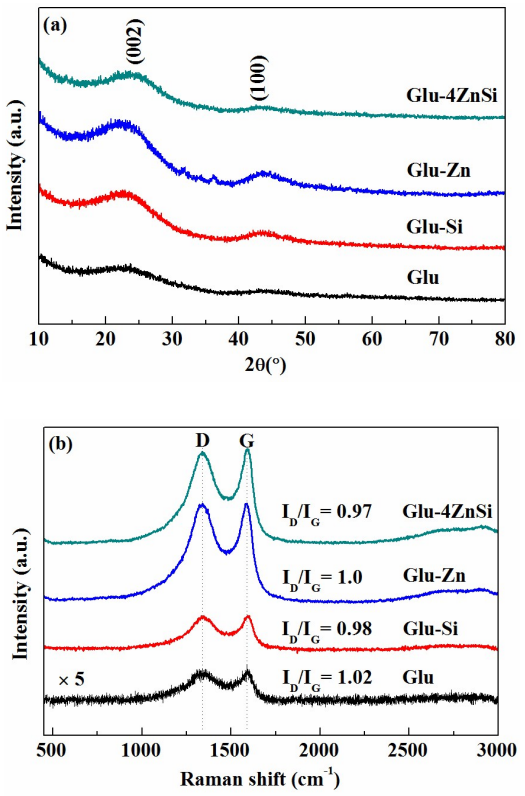

Fig. S3 XRD patterns (a) and Raman spectra (b) of the resultant carbon samples.

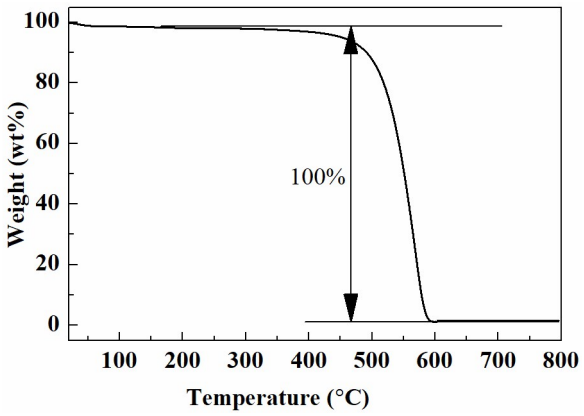

Fig. S4 TG profile of the Glu-4ZnSi sample.

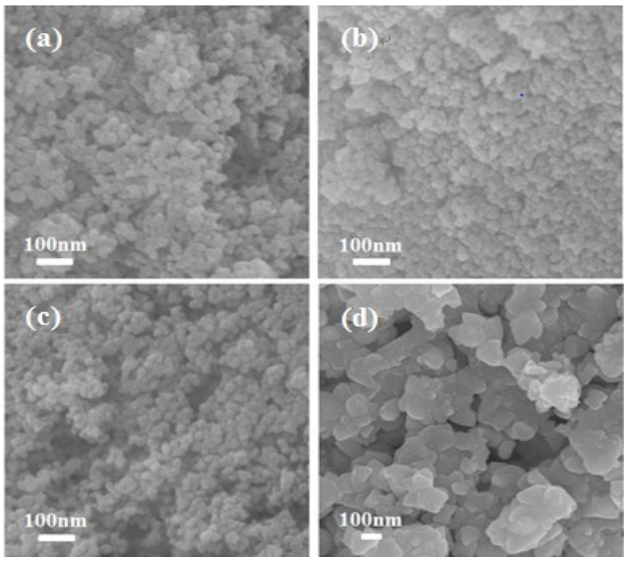

Fig. S5 SEM images of HT-Si (a), HT-Si-$ZnCl_2$ (b), HT-Si-$Zn(NO_3)_2$ (c), and $Zn(CH_3COO)_2$ (d) samples.

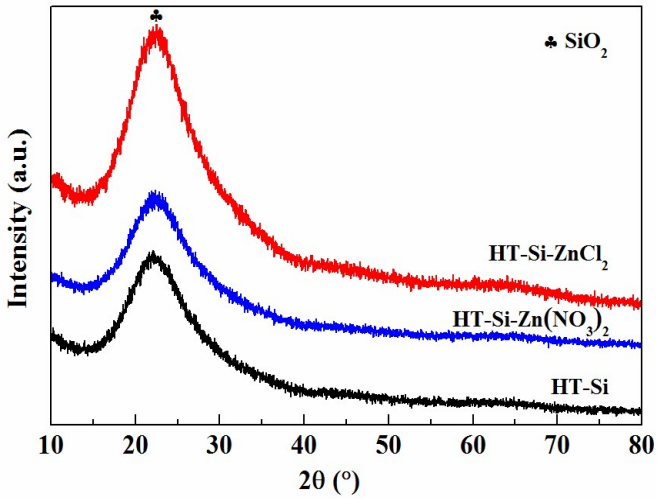

Fig.S6 X-ray diffraction patterns of HT-Si, HT-Si-$Zn(NO_3)_2$ and HT-Si-$ZnCl_2$.

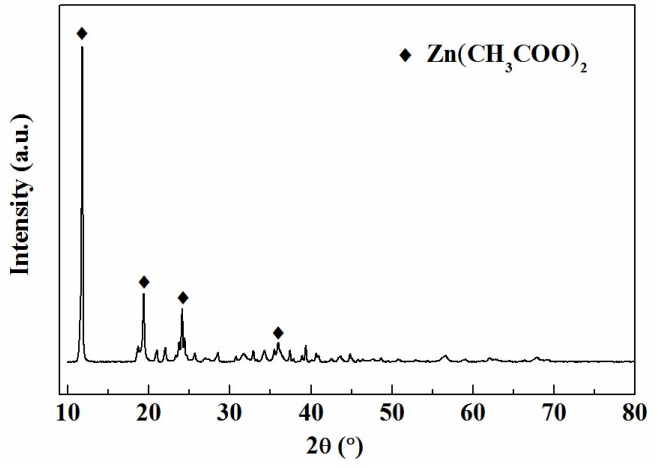

Fig. S7 X-ray diffraction pattern of the $Zn(CH_3COO)_2$ sample.

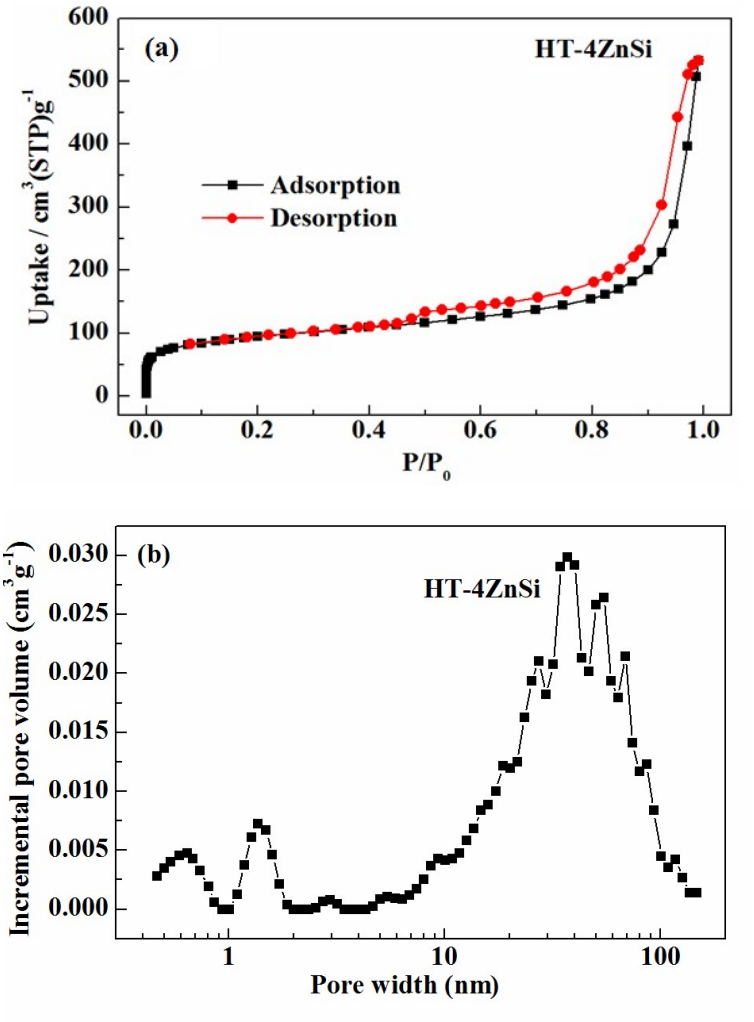

Fig. S8 Nitrogen sorption/desorption isotherms (a) and pore size distributions (b) of HT-4ZnSi sample at 77K.

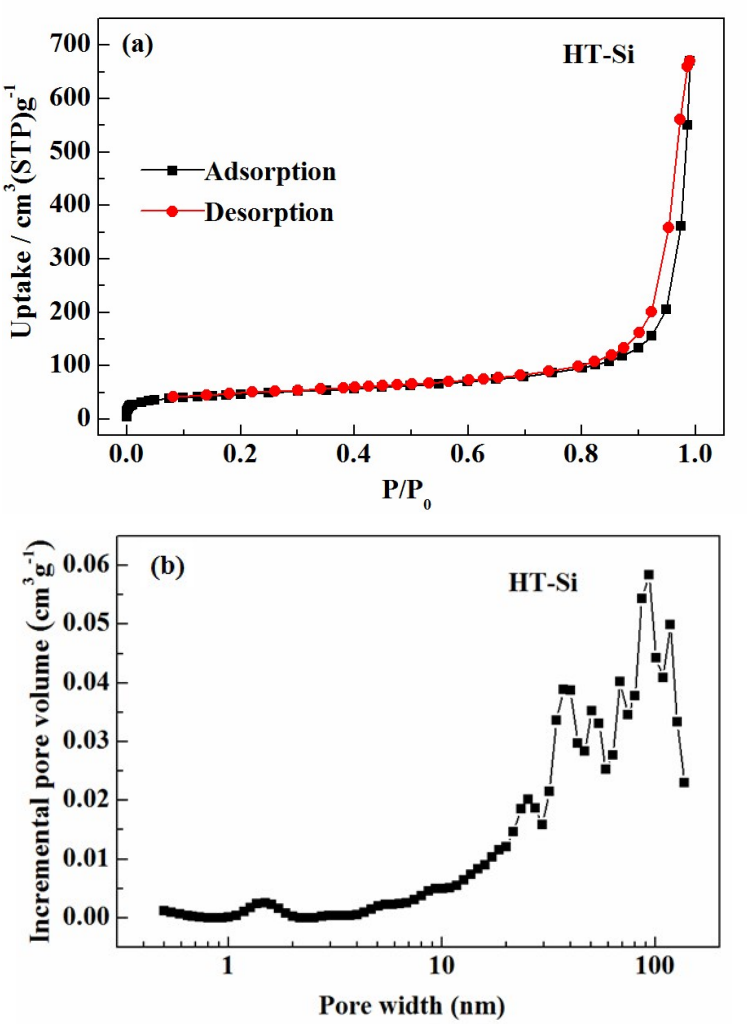

Fig. S9 Nitrogen sorption/desorption isotherms (a) and pore size distributions (b) of HT-Si sample at 77K.

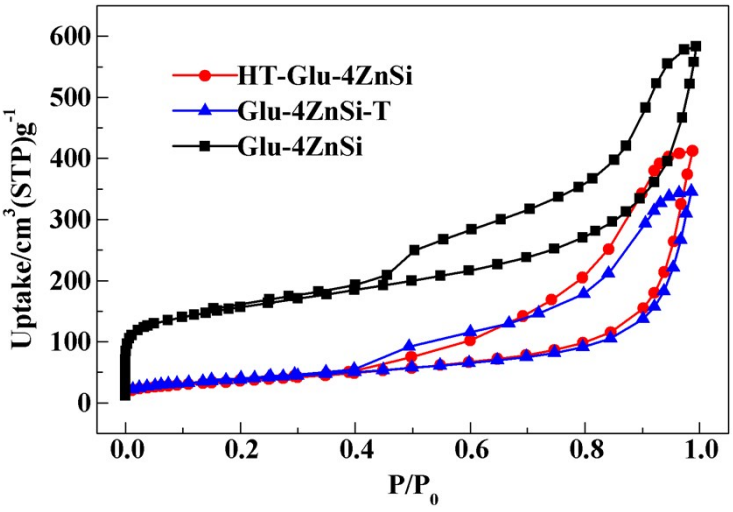

Fig. S10 Nitrogen sorption/desorption isotherms of HT-Glu-4ZnSi, Glu-4ZnSi-T and Glu-4ZnSi samples at 77K.

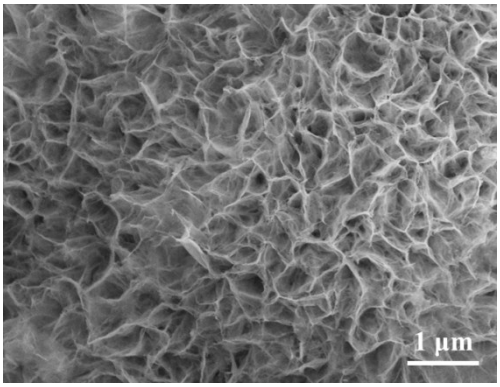

Fig. S11 SEM image of the Glu-4ZnSi-T sample after calcinating at 800 °C in air flow.

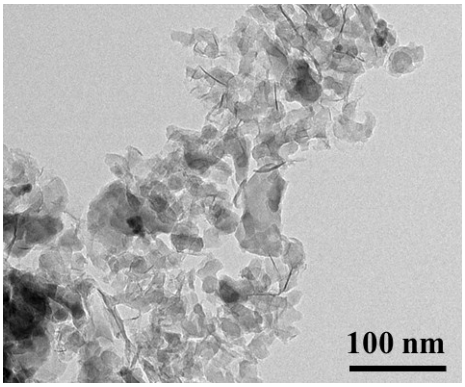

Fig. S12 TEM image of the Glu-4ZnSi-T sample after calcinating at 800 °C in air flow.

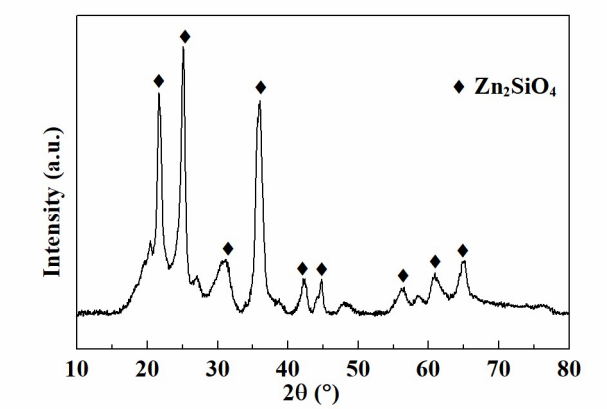

Fig. S13 XRD pattern of the Glu-4ZnSi-T sample after calcinating at 800 °C in air flow.

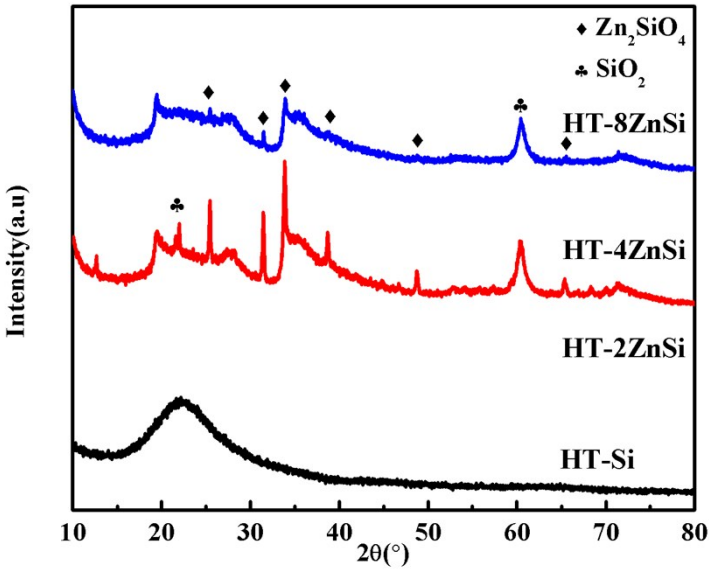

Fig. S14 X-ray diffraction patterns of various HT-ZnSi samples with different Zn/Si ratios.

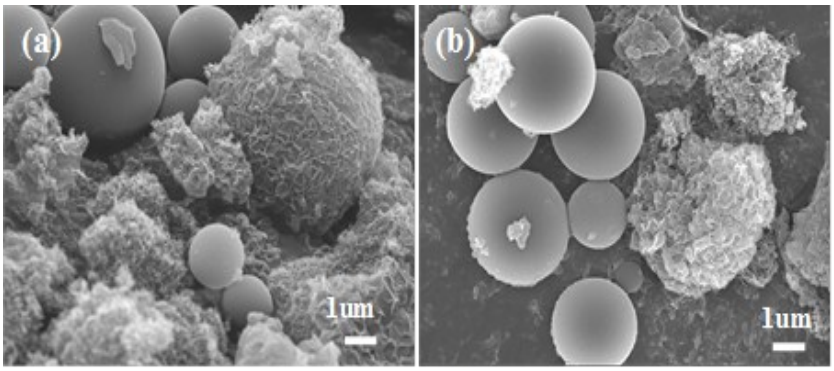

Fig. S15 SEM images of the carbon samples, which were prepared using HT-4ZnSi as the hard template with the glucose concentrations of 0.2 (a) and 0.4 mol/L (b), respectively.

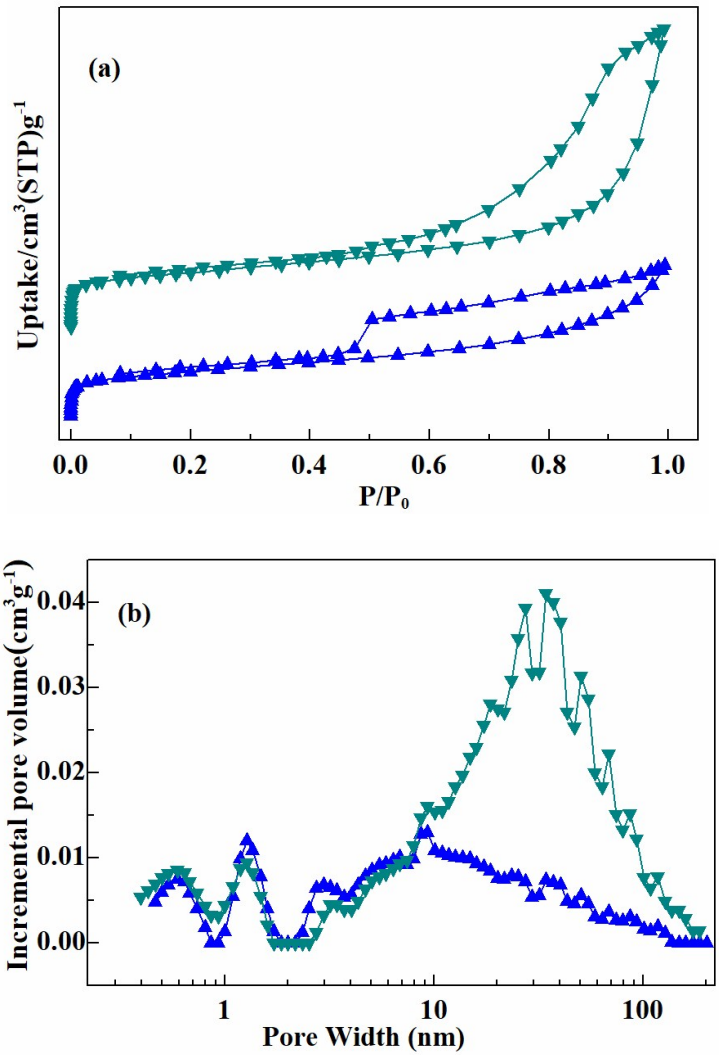

Fig. S16 Nitrogen adsorption/desorption isotherms (a) and pore size distributions (b)) of the resultant carbon nanosheets, which were prepared by the *in situ* self-generating template process with the glucose concentrations of 0.8 (blue) and 1.6 mol/L (green), respectively.

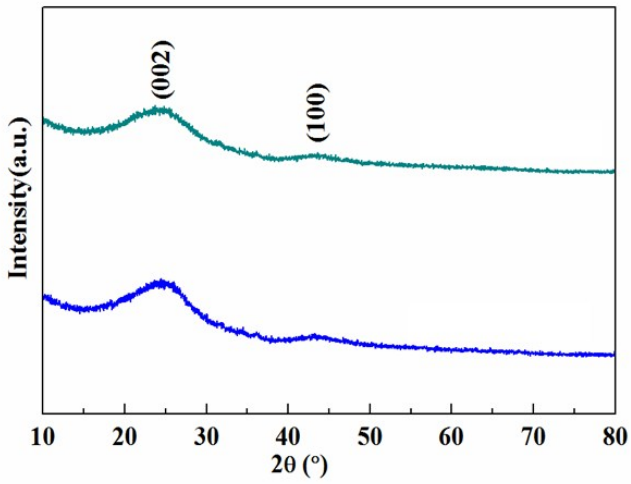

Fig. S17 X-ray diffraction patterns of the resultant carbons, which were prepared by the *in situ*

self-generating template process with the glucose concentrations of 0.8 (blue) and 1.6 mol/L (green), respectively.

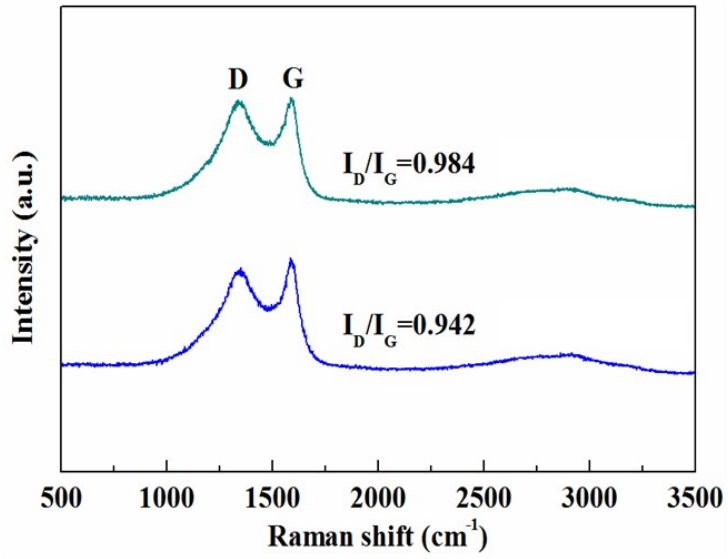

Fig. S18 Raman spectra of the resultant carbons, which were prepared by the *in situ* self-generating template process with the glucose concentrations of 0.8 (blue) and 1.6 mol/L (green), respectively.

Table S1 Yield and elemental analysis data of the carbon materials.

Samples	Yield (wt %)	C (wt %)	H (wt %)	O (wt %)*
Glu	17	88.2	2.3	9.5
Glu-Zn	9	88.4	1.8	9.8
Glu-Si	26	88.1	2.1	9.8
Glu-4ZnSi	14	84.2	2.2	13.6

* Oxygen content was calculated according to the data of carbon and hydrogen atoms.

Table S2 Textural and structural properties of HT-4ZnSi, HT-Glu-4ZnSi, and Glu-4ZnSi-T.

Samples	S_{BET}/m^2 g^{-1}	S_{mic}/m^2 g^{-1}	V_{mic}/V_{total}	V_{total}/cm^3 g^{-1}
HT-4ZnSi	279	91	0.06	0.72
HT-Glu-4ZnSi	133	-	-	0.63
Glu-4ZnSi-T	140	3.5	0.001	0.54

Table S3 Textural and structural properties of HT-Si and two carbon nanosheet samples.

Samples	S_{BET} /m^2 g^{-1}	S_{micro} /m^2 g^{-1}	V_{micro}/V_{total}	V_{total} /cm^3 g^{-1}
HT-Si	169	41	0.61	1.03
Glu-4ZnSi*	485	167	0.10	0.69
Glu-4ZnSi#	591	236	0.07	1.34

* The carbon sample was prepared by the *in situ* self-generating template process with the glucose concentration of 0.8 mol/L; # The carbon sample was prepared by the *in situ* self-generating template process with the glucose concentration of 1.6 mol/L.

Table S4 Average Pd particle diameters and palladium dispersities of Pd/Glu-4ZnSi and Pd/C determined by CO chemisorption data.

Samples	Metal dispersion (%)	Metallic surface area		Active particle diameter (nm)
		m^2/g sample	m^2/g metal	
Pd/Glu-4ZnSi	45.7	2.0	201.2	2.4
Pd/C	34.4	1.5	151.6	3.2